 CMC, vol.28, no.1, pp.57-80, 2012

On the Feedforward Control of Hysteresis for a Piezoelectric Plate

Ligia Munteanu[1] **and Veturia Chiroiu**[1]

Abstract: This paper discusses the modeling and feedforward control of hysteresis in a Cantor-like piezoelectric plate. The generalized play operator is analyzed in connection with the plate equations. Results show that hysteresis can be reduced to less than 40% when applying the feedforward control. The subject of the paper belongs to the field of dynamics, characterization and control at the micro/nanoscale. The choose of the Cantor-like piezoelectric plate is motivated by its special property to generate the subharmonic waves due to the anharmonic coupling between the extended-vibration (phonon) and the localized-mode (fracton) regimes. This behavior is a benefit for several applications to the mechanics of grippers and manipulators at the micro/nano scale. In spite of this, the nonlinearities make the piezoelectric plates lose their accuracy if not controlled. For that, the generalized play operator is connected in this paper to the plate equations and the control is focused on feedforward or compensation technique with no sensor requirement. Such advantage is appreciated in the micro/nano-scale because existing sensors that have the required performances are hardly embeddable. The results have confirmed that feedforward control can give general performances such as accuracy and speed required for this particular application. Such control is of great interest because the costs, sizes, and performances of existing sensors limit their use in this domain.

Keywords: Cantor-like plate, feedforward control, hysteresis operator, subharmonic generation of waves.

1 Introduction

Hysteresis is typically viewed as an undesirable effect in that it complicates the control of the relationship between input and output data in engineering systems. In the 1970s, Krasnoselskii and Pokrovskii studied the concept of hysteresis operator acting in spaces of time dependent functions [Ewing (1885); Kranoselskii and

[1] Institute of Solid Mechanics of Romanian Academy, Ctin Mille 15, Bucharest 010141

Pokrovskii (1983)]. Further researches were developed in a series of works dedicated to hysteresis in connection with PDEs and applicative problems [Brokate and Sprekels (1996); Krečí, (1997); Visintin (1995)]. A useful survey can be found in [Visintin (2002)]. Nonlinear semigroup theory in a Hilbert space was developed by Komura (1967) and extended to Banach spaces by Crandal and Liggett (1871) and Barbu (1976). A survey of basic relevant results from a nonlinear semigroup theory, formulated generally in a Banach space is presented in [Kopfová (2007); Visintin (1993)]. Several models of hysteresis may be represented via rheological models in mechanics by arranging elementary components in series and/or in parallel [Bertotti and Mayergoyz (2006), Mayergoyz, (2003); Bertotti (1998)].

A new approach for inverse control of piezoelectric actuators is presented by Qiu, Jiang and Hu (2011). This new method utilize a modified Prandtl-Ishlinskii model which is based on a combination of two asymmetric hysteresis operators, and the two operators can independently model ascending branches and descending branches of hysteresis loops.

Composite materials such as the fibre-reinforced plates and shells are finding an increasing interest in engineering applications [Cazzani *et al.* (2005)]. Consequently, efficient and robust computational tools are required for the analysis of such structural models.

Such structures are not linear, so the specific nonlinearities can be modeled by the Bouc-Wen or Duhem models or the Preisach models, and so on. But, the unrealistic behavior aspects were found by using the Bouc-Wen model or Duhem models or the Preisach models, with respect to short input signals. The hysteretic loops at the micro/nano scales exhibit the displacement drift, force relaxation and non-closure behavior. The generalized play operator is just one of the models of hysteresis which allows describing of such hysteretic nonlinearities. This model can be easily extended to a generalized discontinuous Prandtl-Ishlinskii operator of play type.

In this paper, the generalized play operator is analyzed in connection with the governing equations of a piezoelectric plate with Cantor-like structure. This structure can be used as actuator or as sensor in several applications in the micro/nano-scale. It is a fact the experimentally evidence of extremely low thresholds for subharmonic generation of waves in 1D artificial piezoelectric plates with Cantor-like structure, as compared to the corresponding homogeneous and periodical plates [Craciun *et al.* (1992); Alippi et al. (1992); Alippi, Craciun and Molinari (1988); Alippi (1982)]. An anharmonic coupling between the extended-vibration (phonon) and the localized-mode (fracton) regimes explained this phenomenon, and also the large enhancement of nonlinear interaction which results from the more favorable frequency and spatial matching of fractons and phonons coupled modes [Chiroiu et al. (2001); Chiroiu, Munteanu and Beldiman (2008)]. When hysteresis is present along with this dynamics, the overall behavior of the piezoelectric plate with Cantor-like structure can be very complex. In order to control this effect, the modeling of the hysteresis has to be as precise as possible [Rakotondrabe (2011)].

The scope of this paper is to model and control the hysteresis phenomenon in piezoelectric plates with Cantor-like structure. The control aspect is focused on feedforward or compensation technique. The main advantage of this control scheme is that no sensor is required. Such advantage is appreciated in the micro/nano-scale because existing sensors that have the required performances are hardly embeddable. The control problem is reduced to a system of differential inclusions and solved. This work is placed in the framework of the Visintin researches on models of hysteresis phenomena and on related PDEs [Visintin (1995, 2002); Mosnegutu and Chiroiu (2010); Teodorescu et al. (2010); Preda et al. (2010); Gliozzi et al. (2010)].

A rate-dependent hysteresis is a hysteresis that has its shape changed when the frequency of the input is changed. Such hysteresis is called dynamic hysteresis. Contrary to a rate-dependent hysteresis, the shape of a rate-independent hysteresis does not change whatever the frequency of the input is. Such hysteresis is called static hysteresis. Usually, it is admitted the separation principle of dynamic hysteresis which states that the dynamic hysteresis can be approximated by a static hysteresis followed by a linear dynamic part [Visintin (2006)]. In this paper, we assume this separation principle. Thus, the modeling and compensation are focused on static hysteresis.

2 Hysteresis Operators

In order to simplify the meaning of the hysteresis, let us consider a system characterized by two scalar variables, the input function $u(t)$ and the output function $w(t)$, confined to a set $L \subset R^2$. $\forall t \in [0,T]$. The function $w(t)$ depends on the previous evolution of $u(t)$ and on the initial state w_0, such as

$$w(t) = A(u,w_0)(t), \quad \forall t \in [0,T], \quad (u(0),w_0) \in L,$$
$$A(u,w_0)(0) = w_0, \tag{2.1}$$

where $A(u,w_0)$ is a memory operator defined in a Banach space of time-dependent functions for any fixed w_0. The memory operator is causal: for $\forall (u_1,w_0),(u_2,w_0)$ with $u_1 = u_2$ in $[0,T]$, then $A(u_1,w_0)(t) = A(u_2,w_0)(t)$.

In the following we present the generalized play operator $w := A(u,w_0) : R^+ \to R$ defined in the sense of Visintin (Fig.1). Let $u(t)$ be any continuous, piecewise linear function on R^+, linear on $[t_{i-1},t_i]$, $i = 1,2,...$ We define $w(t) = A(u,w_0)(t)$ by

$$w(t) = \min\{\gamma_l(u(0)), \max\{\gamma_r(u(0)), w_0\}\}, \text{for } t = 0 \text{ and } w_0 \in R,$$

$$w(t) = \min\{\gamma_l(u(t_i)), \max\{\gamma_r(u(t_i)), w(t_{i-1})\}\}, \text{ for } t \in (t_{i-1}, t_i),\ i = 1, 2, ..., \quad (2.2)$$

where $\gamma_l, \gamma_r : R \to R$ are maximal monotone, possible multivalued functions with

$$\inf \gamma_r(u) \leq \sup \gamma_l(u), \quad \forall u \in R. \quad (2.3)$$

Note that $w(0) = w_0$ only if $\gamma_r(u(0)) \leq w_0 \leq \gamma_l(u(0))$. The classical play operator can be obtained from the general play operator by choosing

$$\gamma_l(u) = u + r,\ \ \gamma_r(u) = u - r, \quad (2.4)$$

with $r \geq 0$ a parameter, $u(t)$ a continuous input function on $[0, T]$ and $w_{r0} \in [-r, r]$ an initial state. Fig. 2 presents the play operator with threshold r. The hysteresis relationship with the PDEs can be written as [Kopfová (2007)]

$$w(x,t) = [A(u(x, ...), w_0(x))](t) \text{ in } Q = \Omega \times [0, T], \quad (2.5)$$

where Ω is a bounded subset of R^n. The generalized play operator is dissipative, in the sense that $||(\lambda I - A)x|| \geq \lambda ||x||$ for $\forall \lambda > 0$, where I is the identity mapping.

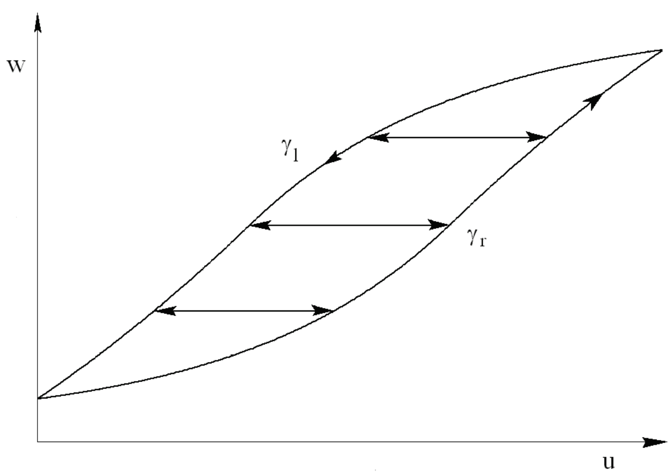

Figure 1: The generalized play operator.

The PDEs with hysteresis can be transformed into systems of differential inclusions. Therefore, the generalized play operator can be defined as a solution in the Sobolev space $W^{1,1}(0,T)$, $w \in W^{1,1}(0,T)$ of a variational inclusion of the type

$$w_{,t} \in \phi(u, w) \text{ in } (0, T),\ w(0) = w_0, \quad (2.6)$$

where comma represents the differentiation with respect to the specified variable. The norm in $W^{1,1}(0,T)$ is defined as

$$||f||_{k,p} = \left(\sum_{i=0}^{k} ||f^{(i)}||_p^p\right)^{1/p} = \left(\sum_{i=0}^{k} \int f^{(i)}|^p \mathrm{d}t\right)^{1/p}.$$

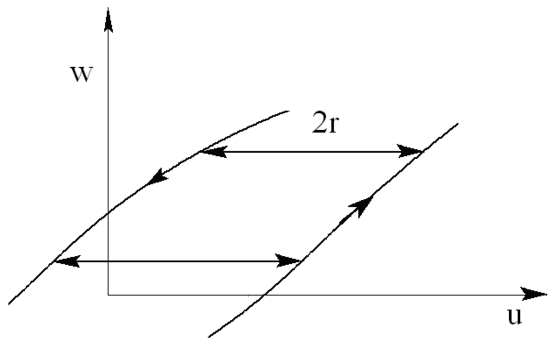

Figure 2: The play operator with threshold r.

The rate-independent differential inclusion is given by

$$w_{,t} \in \phi(u,w) = \begin{cases} \{\infty\} & \text{if } w < \inf \gamma_r(u), \\ [0,+\infty] & \text{if } w \in \gamma_r(u) \backslash \gamma_l(u), \\ \{0\} & \text{if } \sup \gamma_r(u) < w < \inf \gamma_l(u), \\ [-\infty,0] & \text{if } w \in \gamma_l(u) \backslash \gamma_r(u), \\ \{-\infty\} & \text{if } w > \sup \gamma_r(u), \\ [-\infty,+\infty] & \text{if } w \in \gamma_l(u) \cap \gamma_r(u). \end{cases} \tag{2.7}$$

If γ_r and γ_l are Lipschitz-continuous, then the generalized play operator transforms $(u,v) \in W^{1,1}(0,T) \times \mathrm{R}$ into the unique function $w \in W^{1,1}(0,T)$ such that $w(0)$ is the projection of v into $[\gamma_r(u(0), \gamma_l(u(0)]$ and (2.7) is satisfied. The operator can be extended to $C^0([0,T]) \times \mathrm{R}$, and it is equivalent to a variational inequality. We present here one example of PDE with hysteresis [Kopfová (2007)]

$$(u+w)_{,t} - \Delta u = f \text{ in } Q, \tag{2.8}$$

related to a generalized play operator (2.2). Eq,(2.8) is formally equivalent to

$$u_{,t} + \xi - \Delta u = f, \quad w_{,t} - \xi = 0, \quad \xi \in \phi(u,w) \text{ in } Q \tag{2.9}$$

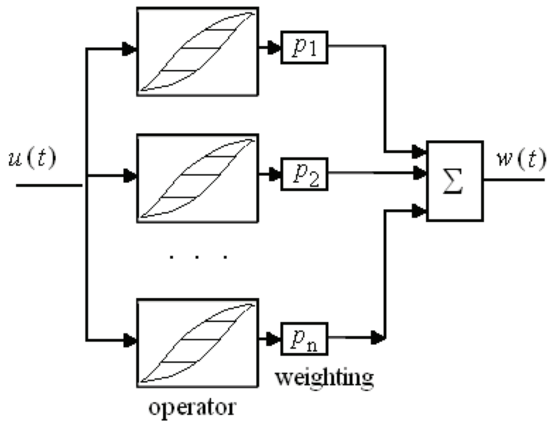

Figure 3: Arrangement in parallel of the hysteresis operators.

where ϕ is defined by (2.7).

The Cauchy problem for (2.9) coupled with homogeneous Dirichlet boundary conditions becomes

$$F \in U_{,t} + A_1 U \text{ in } Q, \quad U(0) = U_0 \text{ in } \Omega, \tag{2.10}$$

where

$$U = (u, w)^T, \quad F = (f, 0)^T,$$

$$A_1 U = (\xi - \Delta u, -\xi)^T, \quad \xi \in \phi(U) \cap R. \tag{2.11}$$

It is well known that a combination in parallel of the hysteresis operators $w := A(u, w_0) : R^+ \to R$ given by (2.2) is used in the practical problems. The block diagram of this combination is presented in Fig. 3.

The model is the sum of the hysteresis operators with weightingsp_i, $i = 1, 2, ..., n$

$$w(t) = \sum_{i=1}^{n} p_i \min\{\gamma_l(u(0)), \max\{\gamma_r(u(0)), w_0\}\} \tag{2.12}$$

for $t = 0$ and $w_0 \in R$,

$$w(t) = \sum_{i=1}^{n} p_i \min\{\gamma_l(u(t_i)), \max\{\gamma_r(u(t_i)), w(t_{i-1})\}\}$$

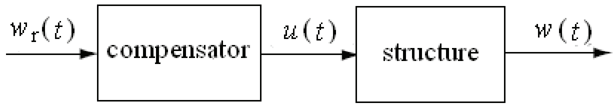

Figure 4: The scheme of the feedforward control.

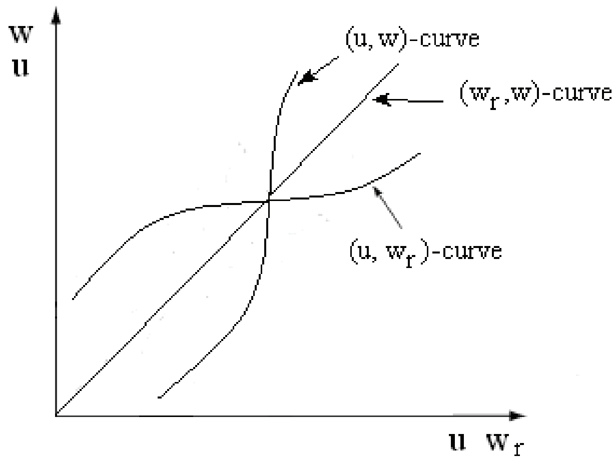

Figure 5: The scheme of compensation of the hysteresis.

for $t \in (t_{i-1}, t_i)$, $i = 1, 2, ...$

Direct hysteresis can be compensated by another hysteresis put in cascade with it. Such scheme is called feedforward control of the hysteresis and it is presented in Fig.4. In the figure, w_r is the reference input to be tracked. Direct hysteresis and its compensator are symmetric relative to the linear curve (w_r, w), as shown in Fig.5. To obtain a linear input-output (w_r, w) with a unit gain, the real system curve (u, w) and the compensator curve (w_r, u) should be symmetric.

This compensator is characterized by thresholds r'_k and the weightings p'_k. The calculation of these parameters follows the principle of Fig.5. The thresholds r'_k, $k = 1, 2, ..., n$, are computed as follow

$$r'_k = \sum_{j=1}^{k} p_j (r_k - r_j), \quad k = 1, 2, ..., n, \tag{2.13}$$

and

$$p'_1 = \frac{1}{p_1}, p'_k = \frac{-p_k}{\left(p_1 + \sum_{j=2}^{k} p_j\right)\left(p_1 + \sum_{j=2}^{k-1} p_j\right)}, \quad k = 2, ..., n. \tag{2.14}$$

The following approach is based on the inverse multiplicative structure scheme and gives the compensator without any additional calculation. The compensator is defined by

$$w(t) = \sum_{i=1}^{n} p_i \min\{\gamma_l(u(0)), \max\{\gamma_r(u(0)), w_0\}\},$$

for $t = 0$ and $w_0 \in R$,

$$w(t) = \sum_{i=1}^{n} p_i \min\{\gamma_l(u(t_{i-1})), \max\{\gamma_r(u(t_{i-1})), w(t_{i-2})\}\} - w_r(t), \tag{2.15}$$

for $t \in (t_{i-2}, t_{i-1}),\ i = 2, 3, ...$

3 The Piezoceramic Plate

The structure is consisting from a composite plate with alternating elements of piezoelectric ceramics (PZ) and an epoxy resin (ER), following a triadic Cantor sequence up to the fourth generation (31 elements (Fig 6) inspired from the papers of Craciun *et al.* (1992); Alippi *et al.* (1992)]. A rectangular coordinate system $Ox_1x_2x_3$ is employed. The origin of the coordinate system $Ox_1x_2x_3$ is located at the left end, in the middle plane of the sample, with the axis Ox_1 in-plane and normal to the layers and Ox_3 out-plane, normal to the plate. The length of the plate is l, the width of the smallest layer is $l/81$ and the thickness of the plate is$h$.

The width of the plate is d. Let the regions occupied by the plate be $V = V^p \cup V^e$ where V^p and V^e are the regions occupied by PZ and ER layers. The boundary surface of V be S partitioned in the following way

$$S = S_1^p \cup S_1^e \cup S_2, \quad S_1^p \cap S_1^e \cap S_2 = 0,$$

where

$S_1^p = \{x_3 = \pm h/2,\ 0 < x_1 < l\}$ is the boundary surface of V^p,

$S_1^e = \{x_3 = \pm h/2,\ 0 < x_1 < l\}$ is the boundary surface of V^e,

and

$S_2 = \{x_1 = 0,\, x_1 = l,\ -h/2 \leq x_3 < h/2\}.$

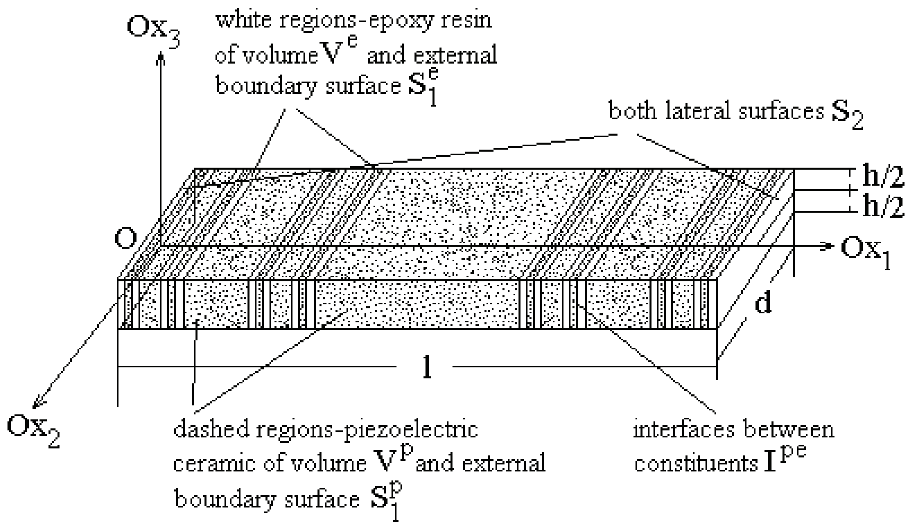

Figure 6: The plate with Cantor-like structure.

Let the unit outward normal of S be n_i the interfaces between constituents be I^{pe}. The existence of multiple fracton and multiple phonon-mode regimes in the displacement field for the structure is proved by Chiroiu *et al.* (2001). We have considered the piezoelectric material to be nonlinear and isotropic, characterized by two second-order elastic constants, three third-order elastic constants, two (linear and nonlinear) dielectric constants and two (linear and nonlinear) coefficients of piezoelectricity. A quantitative knowledge of the second-order material constants is essential for the analysis of the fracton and phonon mode regimes for a piezoelectric plate. The basic equations of interest are given in the following [Zhu *et al.* (2010); Gliozzi *et al.* (2010); Rogacheva (1994); Landau and Lifshitz (1968, 1982); Apte and Ganguli (2009)].

1. The quasistatic motion equations

$$\rho^p \ddot{u}_i = t_{ij,j} \text{ in } V^p, \tag{3.1}$$

$$D_{i,i} = 0, \quad E_i + \varphi_{,i} = 0 \text{ in } V^p, \tag{3.2}$$

where ρ^p is the density, u_i is the displacement vector,t_{ij} is the stress tensor, D_i is the electric induction vector, E_i is the electric field and φ is the electric potential.

2. The constitutive equations

$$\begin{aligned} t_{ij} =&\lambda^p \varepsilon_{kk}\delta_{ij} + 2\mu^p \varepsilon_{ij} + A^p \varepsilon_{il}\varepsilon_{jl} + 3B^p \varepsilon_{kk}\varepsilon_{ij} + C^p \varepsilon_{kk}^2 \delta_{ij} - \\ &- e_k^p E_k \delta_{ij} - \bar{e}_k^p E_k \varepsilon_{ll}\delta_{ij} - \bar{\bar{e}}_k^p E_k \varepsilon_{ll}\delta_{ij} - \bar{\bar{e}}_k^p E_k \varepsilon_{ij} \quad \text{in } V^p, \end{aligned} \tag{3.3}$$

$$D_i = \bar{\varepsilon}^p E_i - \frac{1}{2}\bar{\varepsilon}_i^p E^2 - e_i^p \varepsilon_{kk} - \frac{1}{2}\bar{e}_i^p \varepsilon_{kk}^2 - \frac{1}{2}\bar{\bar{e}}_i^p \varepsilon_{kk}^2 \text{ in } V^p, \tag{3.4}$$

$$\varepsilon_{ij} = \frac{1}{2}(u_{i,j} + u_{j,i} + u_{l.i}u_{l.j}) \text{ in } V, \tag{3.5}$$

where ε_{ij} is the strain tensor, λ^p, μ^p are the Lamé constants, A^p, B^p, C^p are the Landau constants, $\bar{\varepsilon}^p$, $\bar{\varepsilon}_1^p = \bar{\varepsilon}_2^p = \bar{\varepsilon}_3^p$ are the linear and nonlinear dielectric constants, $e_1^p = e_2^p = e_3^p$, $\bar{e}_1^p = \bar{e}_2^p = \bar{e}_3^p$ and $\bar{\bar{e}}_1^p = \bar{\bar{e}}_2^p = \bar{\bar{e}}_3^p$ are the linear and nonlinear coefficients of piezoelectricity and $E^2 = E_1^2 + E_2^2 + E_3^2$.

3. The boundary conditions

$$t_{ij}n_j = \bar{T}_{ij}n_j = \bar{T}_i \text{ on } S_1^p, \tag{3.6}$$

$$D_i n_i = \bar{d}, \quad \varphi = \bar{\varphi} \text{ on } S_1^p, \tag{3.7}$$

where $\bar{T}_i, \bar{d}, \bar{\varphi}$ are quantities prescribed on the boundary and $\bar{T}_{ij}$ is the Maxwell stress tensor. Let us consider that a periodical electric field $\bar{E}_i = \bar{E}_i^0 \exp(\mathrm{i}\omega t)$ is applied to the both surfaces of the plate to excite the Lamb waves, over a wide frequency range. The action of this field is described by Maxwell stress tensor $\bar{T}_{ij}$

$$\bar{T}_{ij} = \frac{1}{4\pi}(\bar{E}_i\bar{E}_j - \frac{1}{2}\bar{E}^2\delta_{ij}) \text{ on } S_1^p. \tag{3.8}$$

The boundary conditions (3.6)-(3.7) on S_1^p are rewritten as

$$t_{13} = \frac{1}{4\pi}\bar{E}_1\bar{E}_3, \quad t_{33} = \frac{1}{8\pi}(\bar{E}_3^2 - \bar{E}_1^2) \text{ on } S_1^p, \tag{3.9}$$

$$D_3 = \bar{E}_3, \quad E_1 = \bar{E}_1 \text{ on } S_1^p. \tag{3.10}$$

For the non-piezoelectric material the governing equations are given by

4. The motion equations

$$\rho^e \ddot{u}_i = t_{ij,j} \text{ in } V^e. \tag{3.11}$$

5. The constitutive equations

$$t_{ij} = \lambda^e \varepsilon_{kk}\delta_{ij} + 2\mu^e \varepsilon_{ij} + A^e \varepsilon_{il}\varepsilon_{jl} + 3B^e \varepsilon_{kk}\varepsilon_{ij} + C^e \varepsilon_{kk}^2 \delta_{ij} \text{ in } V^e. \tag{3.12}$$

6. The boundary conditions

$$t_{ij}n_j = 0 \text{ on } S_1^e, \tag{3.13}$$

or

$$t_{13} = 0, \quad t_{33} = 0 \text{ on } S_1^p. \tag{3.14}$$

7. The boundary conditions on S_2

$$-u_1 = -u_3 = 0. \tag{3.15}$$

8. The conditions on interfaces between constituentsI^{pe}. At the interfaces between constituents the displacement and the traction vectors are continuous

$$[u_1] = [u_3] = 0, \quad [t_{11}] = [t_{13}] = 0 \text{ on } I^{pe}, \tag{3.16}$$

where the bracket indicates a jump across the interface and $k = 1,3$. The equations with hysteresis result by coupling Eqs. (3.1)-(3.16) with the parallel arrangement of generalized play operators presented in Fig.3

$$\rho^p u_{,itt} + \xi_i = t_{ij,j}, \quad w_{,itt} - \xi_i = 0,$$

$$\xi_i \in \phi(u,w) \text{ in } V^p \tag{3.17}$$

$$\rho^e u_{,itt} + \xi_i = t_{ij,j}, \quad w_{itt} - \xi_i = 0,$$

$$\xi_i \in \phi(u,w) \text{ in } V^e, \tag{3.18}$$

where ϕ is defined by (2.7).

In order to present the results of applying the hysteresis compensator (2.15), we start with the resonant vibration modes excited by applying an external electric field $\bar{E}^1 = \bar{E}_3 = \bar{E}^0 \exp(\mathrm{i}\omega_0 t)$ on both sides of the plate with$\omega = \omega_n$. If $\bar{E}^0$ is increased above a threshold value $\bar{E}_{th}^0$ =5.77V the $\omega/2$ subharmonic generation is observed. Note that Alippi *et. al*. (1992) obtain in the Cantor-like sample typical values of the lowest threshold voltages of 3-5V. The amplitude of waves is calculated at the surface of the plate as a function of $\bar{E}^0$. Figs.7 and 8 show the displacements of the normal modes $\omega/2\pi$=0.332MHz, 0.550MHz and respectively of the subharmonic modes $\omega/4\pi$=166MHz, 0.275MHz. Two kinds of vibration regimes are found: a localised-mode (fracton) regime represented in Fig.9 for $\omega/2\pi$=1.223MHz, 1.964MHz and 2.340MHz, and an extended-vibration (phonon) regime represented in Fig.10 for $\omega/2\pi$= 3.109MHz and 3.422MHz. A sketch of the plate geometry is given on the abscissa (dashed, piezoelectric ceramic and white, epoxy resin.

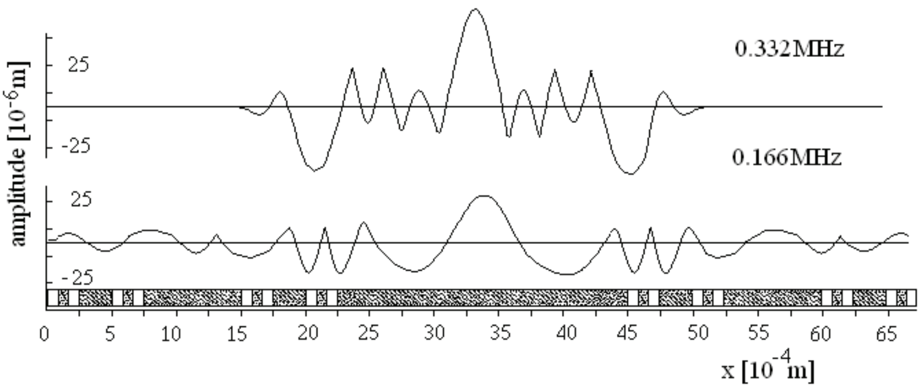

Figure 7: Amplitudes of the surface displacement of the normal mode $\omega/2\pi$= 0.332MHz and the subharmonic mode $\omega/4\pi$=0.166MHz

The fracton vibrations are mostly localised on a few elements, while the phonon vibrations essentially extend to the whole plate. In the case of a periodical plate the dispersion prevents good frequency matching between the fundamental and appropriate subharmonic modes. For the homogeneous plate the mismatch $\omega_n - \omega/2$ is due to the symmetry of fundamental modes with respect to x. Only symmetric odd n can induce a subharmonic, but never $\omega/2$ coincides with a plate vibration mode.

For a Cantor-like plate, we have obtained qualitatively the same result as Craciun *et al.* (1992): given a normal mode ω_n, for excitation at $\omega = \omega_n$, the value of the expected threshold i. e. the ability of generating the $\omega/2$ subharmonic, is determined by the existence of a normal mode with: (i) small frequency mismatch $\omega_n - \omega/2$, and, (ii) large spatial overlap between the fundamental and subharmonic displacement field.

The behavior of the Cantor-like plate is accompanied by the hysteresis phenomenon which may leads to degradation of the motion by driving it to limit-cycle instability.

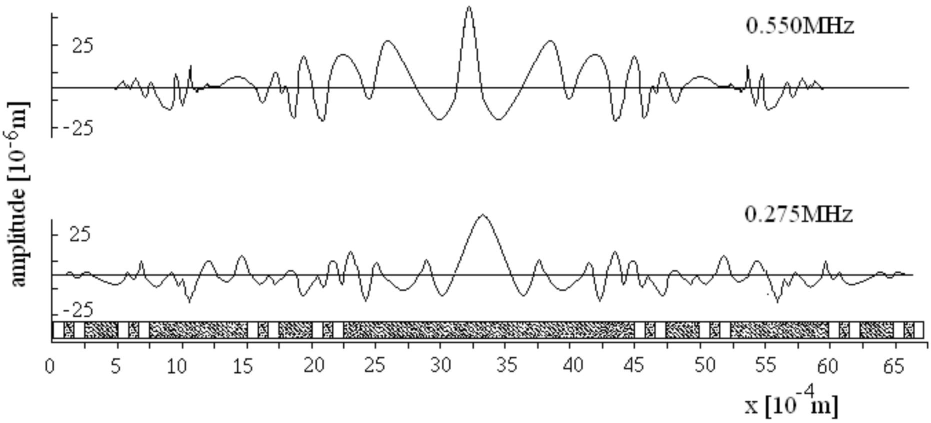

Figure 8: Amplitudes of the surface displacement of the normal mode $\omega/2\pi$= 0.550MHz and the subharmonic mode $\omega/4\pi$=0.275MHz.

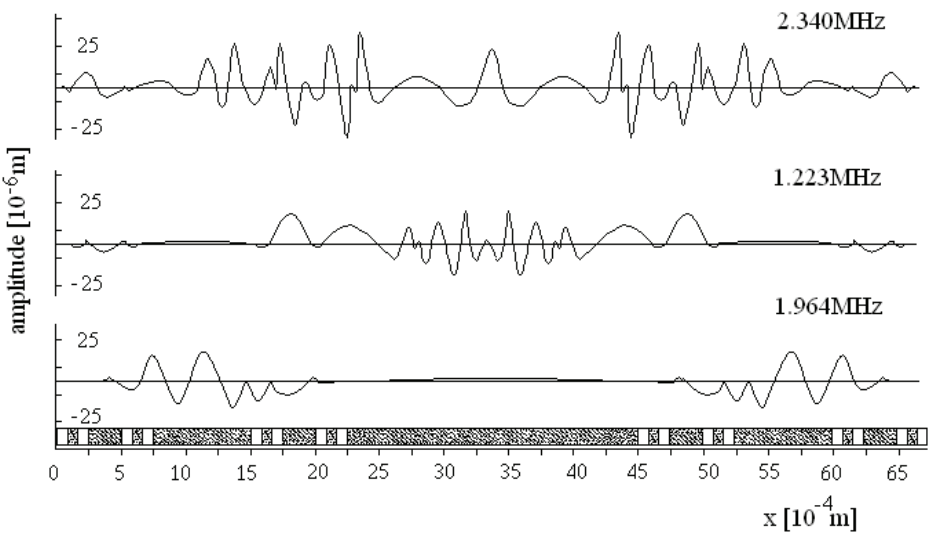

Figure 9: The normal amplitudes for three localised vibration modes ($\omega/2\pi$=1.223MHz, 1.964MHz and 2.340MHz).

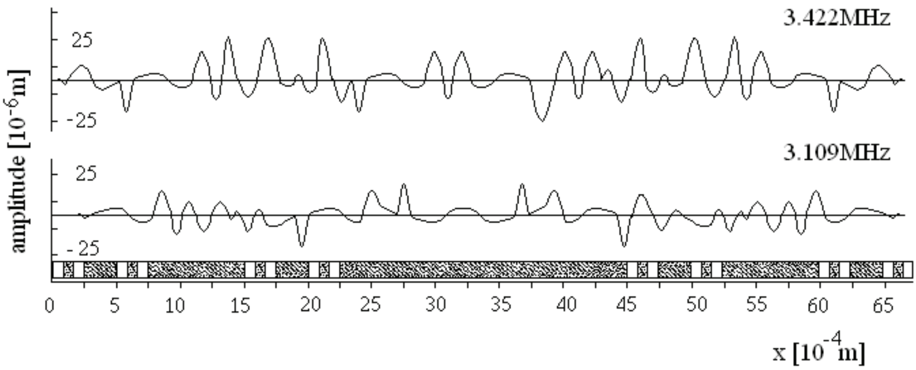

Figure 10: The normal amplitudes for two extended vibration modes ($\omega/2\pi$=3.109MHz and 3.422MHz.

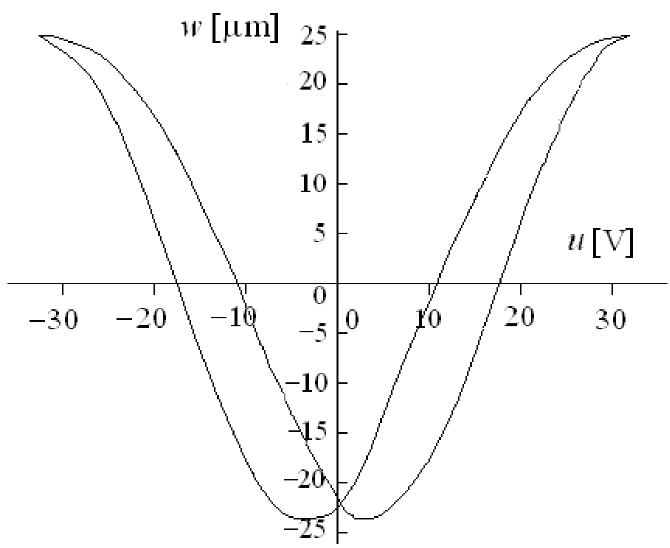

Figure 11: Hysteresis loop for the Cantor like plate.

Fig.11 represents the hysteresis behavior of the plate. The loop is independent of frequency. The control problem is applied next by using the hysteresis compensator (2.15). The aim is to clearly show the contribution of this compensator.

The energy dissipation, i.e. the damping capacity ΔW per unit mass, in one cycle,

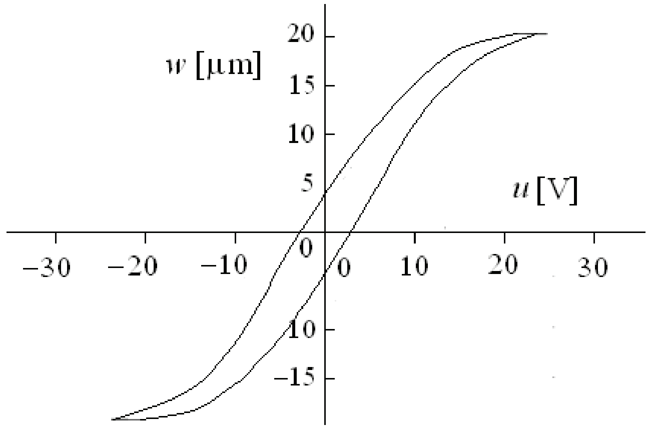

Figure 12: Output w versus the reference input, when the hysteresis compensator is used.

is given by the net work done by the damping force f_d, i.e.

$$\Delta W = \int f_d(x,t)\mathrm{d}x = \int_{-\varphi/\omega}^{(2\pi-\varphi)\omega} f_d \dot{x}\mathrm{d}t, \tag{3.19}$$

where φ is the response phase, $x = DV$ is the displacement, V is the voltage, and D is a dimensional constant done by the relationship between the bending moment and the applied voltage. The damping force is calculated as follows [Donescu, Chiroiu and Munteanu (2009)]

$$f_d(x,t) = \int_V \int_{-\infty}^{t} C(x,\xi,t-\tau)\frac{\partial w(\xi,\tau)}{\partial t}\mathrm{d}\tau\mathrm{d}\xi, \tag{3.20}$$

with

$$C(x,\xi,t-\tau) = H(x)\frac{\alpha}{2}\exp\left(-\alpha\frac{1+\tilde{\nu}}{\tilde{E}}|x-\xi|\right)\delta(t-\tau), \tag{3.21}$$

where $H(x)$ is the Heaviside function, δ is the delta function, α is a constant, $\tilde{E}$ is the Young elasticity modulus of the Cantor like material, computed as

$$\tilde{E} = \frac{\tilde{\rho}\tilde{c}_2^2(3\tilde{c}_1^2 - 4\tilde{c}_2^2)}{\tilde{c}_1^2 - \tilde{c}_2^2}, \tag{3.22}$$

with $\tilde{c}_1$ and $\tilde{c}_2$, the longitudinal and shear wave speeds, respectively. The Poisson's ratio of the Cantor like material is given by

$$\tilde{\nu} = \frac{\tilde{c}_1^2 - 2\tilde{c}_2^2}{2(\tilde{c}_1^2 - \tilde{c}_2^2)}. \tag{3.23}$$

Expression (3.20) represents the general form of nonlocal damping model. The Heaviside function $H(x)$ denotes the presence of nonlocal damping.

The output w versus the reference input u is illustrated in Fig.12. By using (3.19)-(3.23) with α =0.255, it results that $\frac{\Delta W_{control}}{\Delta W} = 0.40019$. This results show that hysteresis can be reduced to less than 40% when applying the feedforward control. Such control can improve the performance of the Cantor-like plate dedicated to the micromanipulation tasks.

4 Micromanipulator Using the Cantor Plate

In order to prove that proposed method really improve the performances, let us simulate the behavior of a micromanipulator having the task of insertion of peg-in hole for micro assembly operations [Jain, Patkar and Majumdar (2009)]. The micromanipulator has three fingers consisted from thin cantilever Cantor strips (40mm$\times$10mm$\times$0.2mm) for holding various objects and a top lifting thick link (40mm$\times$10mm$\times$2mm) (see Fig. 13).

The manipulator has f degrees of freedom, $f = f_r + f_e$, with $f_r = 6$ the rigid body degrees of freedom due to the wrist motion, and $f_e = \sum_{i=1}^{3} f_{ei}$, the elastic degrees of freedom depending on the modeling accuracy. Let introduce the vector of generalized coordinates $q = [q_r^T, q_e^T]^T$, where $q_r = [\beta_0, s]^T$, $\beta_0$the rotation about the vertical axis and s the local joint displacement of the wrist

The flexible finger is modeled as a Euler-Bernoulli beam with a moment applied at the free end (Fig. 14) (Hiller and Schneider (1997)].. The relationship between the bending moment M and the curvature of the beam κ is expressed as M $= \frac{\kappa d h^3 \tilde{E}}{12}$, where d and h are the width and the thickness of the beam, respectively. The relationship between κ and the voltage V is $\kappa = kV$, with ka constant. The wave speeds $\tilde{c}_1$ and $\tilde{c}_2$ have the values 6.298mm/μs, and 3.249mm/μs. The density $\tilde{\rho}$ has the value 7.369 g/ml.

The introducing peg-in-hole operation needs to suppose that the axis of the peg coincides with the axis of the hole (lateral alignment) or if the axis of the peg does not coincide with the hole axis, both axis have to be parallel to each other.

The generalized coordinates for each elastic finger $i = 1,2,3$ is $q_{ei} = [q_{u_2 i}, q_{u_3 i}, q_{\alpha i}]^T$.

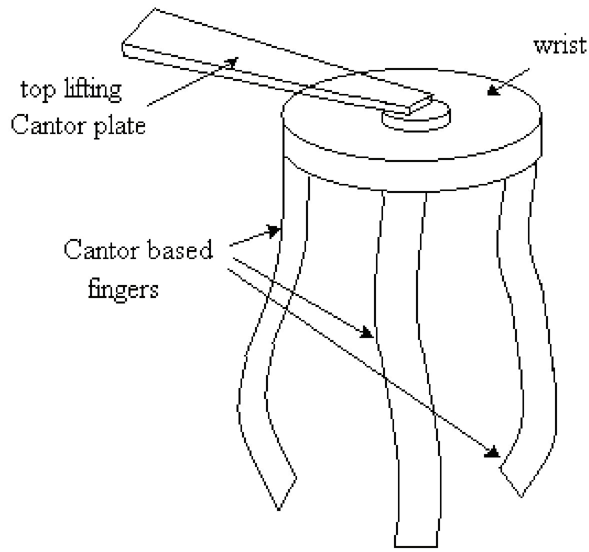

Figure 13: Micromanipulator with Cantor-like structure.

The displacement and angles vectors which measure the lateral and angular misalignment are denoted by $U = [u_1, u_2, u_3]^T$ and $\varphi = [\alpha, \beta, \gamma]^T$, respectively.

Let K_0 be the initial reference frame of the system, K the input reference frame and K' the output frame (Fig 15a) [Hiller and Schneider (1997)]. The elastic transmission mechanism of the position (R, r), velocity$\bar{V}$, acceleration $\dot{V}$ and the force F fields, from K to K', are described next [Lascu *et al.* (2004); Hiller and Schneider (1997); Lee *et al.* (2008)]

$$R' = R \cdot \Delta R, \quad \Delta R = I + \varphi, \tag{4.1}$$

$$r' = \Delta R^T r + \Delta r, \quad \Delta r = \Delta R^T (x + U), \tag{4.2}$$

$$\bar{V} = \begin{bmatrix} \omega' \\ v' \end{bmatrix} = \begin{bmatrix} \Delta R^T & 0 & \Delta R^T \Phi_R \\ -\Delta r \Delta R^T & 0 & \Delta R^T \Phi_T \end{bmatrix} \begin{bmatrix} \omega \\ v \\ \dot{q}_e \end{bmatrix}, \tag{4.3}$$

$$\dot{V} = \begin{bmatrix} \dot{\omega}' \\ a' \end{bmatrix} = \begin{bmatrix} \Delta R^T & 0 & \Delta R^T \Phi_R \\ -\Delta r \Delta R^T & 0 & \Delta R^T \Phi_T \end{bmatrix} \begin{bmatrix} \dot{\omega} \\ a \\ \ddot{q}_e \end{bmatrix} + \begin{bmatrix} \varepsilon_\omega \\ \varepsilon_a \end{bmatrix}, \tag{4.4}$$

$$F=\begin{bmatrix}\tau\\ f\\ Q_e\end{bmatrix}=\begin{bmatrix}\Delta R & \Delta R\Delta r\\ 0 & \Delta R\\ \Phi_R^T\Delta R & \Phi_T^T\Delta R\end{bmatrix}\begin{bmatrix}\tau'\\ f'\end{bmatrix}, \tag{4.5}$$

where $\varepsilon_\omega=\omega'\times\dot\theta$ and $\varepsilon_a=\Delta R^T\omega\times(s\omega'\times U+2\dot sU)$, and

$$U=\Phi_T q_e,\quad \varphi=\Phi_R q_e, \tag{4.6}$$

$$\Phi_{Ti}(x)=A_{Ti}x+B_{Ti}x^2\ +C_{Ti}x^3,\quad i=1,2..., \tag{4.7}$$

$$\Phi_{Ri}(x)=A_{Ri}x+B_{Ri}x^2\ +C_{Ri}x^3,\quad i=1,2..., \tag{4.8}$$

whereA_i,B_i,C_i are unknown constants. Fig.15b shows the evolution of the motion from K to K'. For simplicity, let us suppose that the axis of K, K' coincide with the axis U.

Eqs. (4.1)-(4.5) become [Hiller and Schneider (1997)]

$$R'=R\cdot\Delta R,\quad \Delta R=I+U\sin\theta+(1-\cos\theta)U^2, \tag{4.9}$$

$$r'=\Delta R^T r+Us, \tag{4.10}$$

$$\bar V=\begin{bmatrix}\omega'\\ v'\end{bmatrix}=\begin{bmatrix}\Delta R^T & 0 & U & 0\\ -\Delta r\Delta R^T & \Delta R^T & 0 & U\end{bmatrix}\begin{bmatrix}\omega\\ v\\ \dot\theta\\ \dot s\end{bmatrix}, \tag{4.11}$$

$$\dot{\bar V}=\begin{bmatrix}\dot\omega'\\ a'\end{bmatrix}=\begin{bmatrix}\Delta R^T & 0 & U & 0\\ -\Delta r\Delta R^T & \Delta R^T & 0 & U\end{bmatrix}\begin{bmatrix}\omega\\ v\\ \dot\theta\\ \dot s\end{bmatrix}+\begin{bmatrix}\varepsilon_\omega\\ \varepsilon_a\end{bmatrix}, \tag{4.12}$$

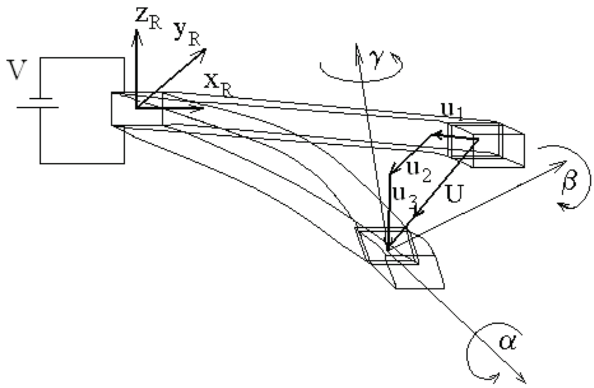

Figure 14: Euler-Bernoulli flexible finger.

$$F = \begin{bmatrix} \tau \\ f \\ Q_e \end{bmatrix} = \begin{bmatrix} \Delta R & \Delta R \Delta r \\ 0 & \Delta R \\ \Phi_R^T \Delta R & \Phi_T^T \Delta R \end{bmatrix} \begin{bmatrix} \tau' \\ f' \end{bmatrix} \quad . \tag{4.13}$$

Finally, the motion equations are given by [Hiller and Schneider (1997)]

$$M(q)(\ddot{q}+\dot{\xi})+g(q,\dot{q}+\xi)=h(q,\dot{q}+\xi)+G(q)\vartheta=0, \tag{4.14}$$

where $\dot{w}-\xi=0$, M is the symmetric, positive-definite inertia matrix, g is the vector of the generalized centrifugal forces, h the vector of the generalized applied voltage, and ϑ the vector of driving forces and torques

$$\vartheta = F_R = [\tau_0, F_{vol}]^T, \tag{4.15}$$

whereτ_0 is the driving torque at the wrist, and $F_{vol}$the resulting driving force due to the applied voltage.

The matrix G describes the mapping of $\vartheta$to generalized forces

$$G\vartheta = [F_R^T, 0^T]^T. \tag{4.16}$$

Starting from an initial configuration without any deflections we can calculate both fields $U=[u_1,u_2,u_3]^T$ and $\varphi=[\alpha,\beta,\gamma]^T$ with respect to time, respectively.

Numerical simulation was carried out for the material constants shown in Table 1. We have paid attention on the accurate numerical model to avoid erroneous parameter estimates.

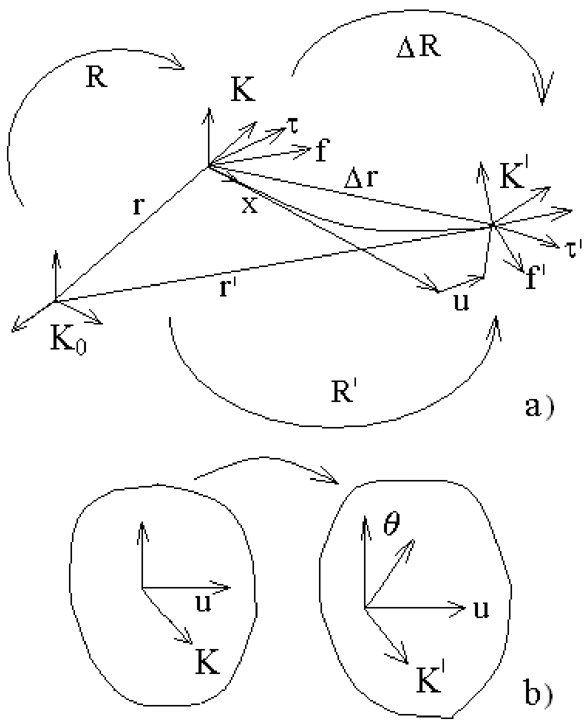

Figure 15: References frames.

Table 1: The material constants for piezoelectric ceramics and epoxy resin [Chiroiu *et al*. 2001].

	piezoelectric ceramics	epoxy resin
	71.6 GPa	42.31 GPa
	35.8 GPa	3.76 GPa
	-2000GPa	2.8 GPa
	-1134GPa	9.7 GPa
	-900GPa	-5.7GPa
	4.065 nF/m	-
	2.079 nF/m	-
	-0.218nm/V	-
=	-0.435nm/V	-
	7650 kg/m	1170kg/m

Performance of the insertion depth of micromanipulator with respect to the voltage is displayed in Fig.16 for without and with the hysteresis compensator.

The energy dissipation, i.e. the damping capacity ΔW per unit mass, in one cycle, is given by (3.19). By using (3.19)-(3.23) with α =0.255, and $D = \frac{\kappa d h^3 \tilde{E}}{12} \frac{1}{F_{tot}\cos\beta}$, we obtain $\frac{\Delta W_{control}}{\Delta W} = 0.39919$. This results show that hysteresis can be reduced to less than 40% when applying the feedforward control.

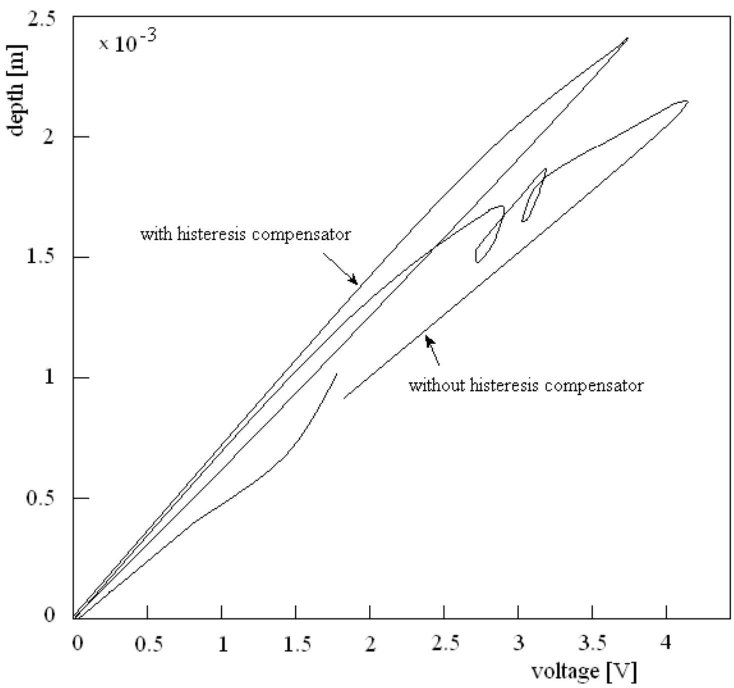

Figure 16: Output depth versus the voltage, without and with the hysteresis compensator.

5 Results and Conclusion

The paper's objective originates in the difficulty to integrate sensors in the control issues of micro / nano world. This means that in this world the open-loop control should solve the problems solved normally by the closed-loop control. In this context, the accuracy of the mathematical model is decisive to synthesize the consistent and effective open loop control procedures (with no feedback so).

The Cantor like piezoelectric structure exhibits large bending or stretching with electrical stimuli, due to the property to generate the subharmonic waves by the anharmonic coupling between the extended-vibration (phonon) and the localized-mode (fracton) regimes. The generalized play operator is connected in this paper to the motion equations of the micromanipulator having the task of insertion of peg-in hole for micro assembly operations. The control is focused on feedforward or compensation technique with no sensor requirement. The Cantor like material facilitates the insertion of peg-in-hole for micro assembly operations. The results have confirmed that feedforward control can give interesting performances such as accuracy and speed required for this particular application. Results show that hysteresis can be reduced to less than 40% when applying the feedforward control.

References

Alippi, A. (1982): Nonlinear acoustic propagation in piezoelectric crystals. *Ferroelectrics* 42: 109–116.

Alippi, A.; Craciun, F.; Molinari, E. (1988): Stopband edges in the dispersion curves of Lamb waves propagating in piezoelectric periodical structures. *Applied Physics Letters* 53(19):1806.

Alippi, A.; Shkerdin, G.; Berttucci, A.; Craciun, F.; Molinari, E.; Petri, A. (1992): Threshold lowering for subharmonic generation in Cantor composite structures. *Physica A* 191(1-4): 540–544.

Barbu, V. (1976): Nonlinear semigroups and differential equations in Banach spaces. Noordhoff, Leyden, 1976.

Bertotti, G. (1998): Hysteresis in Magnetism. Academic Press, Boston.

Bertotti, G.; Mayergoyz, I. (eds.) (2006): The Science of Hysteresis. Elsevier, Amsterdam.

Brokate, M.; Sprekels, J. (1998): Hysteresis and Phase Transitions. Springer, Berlin 1996.

Chiroiu, V.; Delsanto, P.P.; Scalerandi, M.; Chiroiu, C.; Sireteanu, T. (2001): Subharmonic generation in piezoelectrics with Cantor-like structure. *Journal of Physics D: Applied Physics, Institute of Physics Publishing* 34(3): 1579–1586.

Chiroiu, V.; Munteanu, L.; Beldiman, M. (2008): Bucklewaves in piezoelectrics with Cantor like structure. *The International Review of Mechanical Engineering* (IREME), 2(3): 122–133.

Craciun, F.; Bettucci, A.; Molinari, E.; Petri, A.; Alippi, A. (1992): Direct experimental observation of fracton mode patterns in one-dimensional Cantor composites. *Phys. Rev. Lett*. 68 (10).

Crandall, M.C.; Liggett, T.M. (1971): Generation of semigroups of nonlinear transformations on general Banach spaces. *Amer. J. Math*. 93: 265–298.

Donescu, St.; Chiroiu,V.; Munteanu, L. (2009): On the Young's modulus of an auxetic composite structure, *Mechanics Research Communications* 36: 294–301.

Ewing, J.A. (1885): Experimental Research in Magnetism. *Philosophical Transactions of the Royal Society of London* 176 (II).

Gliozzi, A.S.; Munteanu, L.; Sireteanu, T.; Chiroiu, V. (2010) : An identification problem from input-output data. *Revue Roumaine des Sciences Techniques, série de Mécanique Appliquée*, 55(3).

Hiller, M.; Schneider, M. (1997): Modelling, simulation and control of flexible manipulators, *European Journal of Mechanic- A/Solids* 16:127–150.

Jain, R.K.; Patkar, U.S.; Majumdar, S. (2009): Micro gripper for micromanipulation using IPMCs (ionic polymer metal composites). *Journal of Scientific & Industrial Research*, 68:23–28.

Komura, Y. (1967): Nonlinear semi-groups in Hilbert space. *Journal of the Mathematical Society of Japan* 19(4): 493–507.

Kopfová, J. (2007): Nonlinear semigroup methods in problems with hysteresis. *Discrete and Continuous Dynamical Systems Supplement* 580–589.

Kranoselskii, M.A.; Pokrovskii, A.V. (1983): Systems with Hysteresis, Springer, Berlin (Russian ed. Nauka, Moscow 1983).

Krečí, P. (1997): Convexity, Hysteresis and Dissipation in Hyperbolic Equations. Gakkotosho, Tokyo.

Landau, L.D.; Lifshitz, E.M. (1968): Theory of Elasticity, Moscow.

Landau, L.D.; Lifshitz, E.M. (1982): Electrodynamics of Continuous Media, Moscow.

Lascu, V.G.; Chiroiu, V.; Nicolescu, C.M.; Munteanu, L. (2004): Application of the genetic algorithm for solving the dynamic equations of a flexible manipulator, *Revue Roumaine des Sciences Techniqués, serie de Mecanique Appliquée* 49 (1-6): 25–37.

Lee, S.Y.; Lu, S.Y.; Liu, Y.R.; Huang, H.C. (2008): Exact large deflection solutions for Timoshenko beams with nonlinear boundary conditions. *CMES: Computer Modeling in Engineering & Sciences*, 33: 293–312.

Mayergoyz, I.D. (2003): Mathematical Models of Hysteresis and Their Applications. Elsevier, Amsterdam.

Mosnegutu, V.; Chiroiu, V. (2010): On the dynamics of systems with friction. *Proc. of the Romanian Academy, Series A: Mathematics, Physics, Technical Sci-*

ences, Information Science, 11(1).

Preda, V.; Ionescu, M.F.; Chiroiu, V.; Sireteanu, T. (2010) : A Preisach model for the analysis of the hysteretic phenomena. *Revue Roumaine des Sciences Techniques, série de Mécanique Appliquée*, 55(3).

Rakotondrabe, M. (2011): Bouc-Wen modeling and inverse multiplicative structure to compensate hysteresis nonlinearity in piezoelectric actuators. *IEEE - Transactions on Automation Science and Engineering* (TASE), 8(2): 428–431.

Rogacheva, N.N. (1994): The Theory of Piezoelectric Shells and Plates, CRC Press, Boca Raton.

Teodorescu, P.P.; Chiroiu, V.; Munteanu, L.; Dumitriu, D. (2010): On the resonance wave interaction phenomenon. *Revue Roumaine des Sciences Techniques, série de Mécanique Appliquée* 55(1), 31–38.

Visintin, A. (1993): Hysteresis and semigroups, in *Models of Hysteresis*, A.Visintin, ed., Longman, Harlow 192–206.

Visintin, A. (1995): Differential Models of Hysteresis. Springer-Verlag, Berlin 1995.

Visintin, A. (2002): Quasi-linear hyperbolic equations with hysteresis. *Ann. Inst. H. Poincaré, Nonlinear Analysis* 19: 451–476.

Visintin, A. (2006): Mathematical models of hysteresis, In: *The Science of Hysteresis* (G. Bertotti, I. Mayergoyz, eds.) Elsevier 1: 1–123.

Zhu, H.H.; Cai, Y.C.; Paik, J.K.; Atluri, S.N. (2010): Locking-free thick-thin rod/beam element based on a von Karman type nonlinear theory in rotated reference frames for large defomation analyses of space-frame structures. *CMES: Computer Modeling in Engineering & Sciences* 57(2): 175–204.

Wen P.H.; Hon Y.C. (2007): Geometrically nonlinear analysis of Reissner-Mindlin plate by meshless computation. *CMES: Computer Modeling in Engineering & Sciences* 21: 177–191.